

## Nanoporous Fullerene Nanowhiskers

M. Sathish,\*<sup>†</sup> K. Miyazawa,<sup>†</sup> and T. Sasaki<sup>‡</sup>

Fuel Cell Materials Center, Nano-ionics Materials Group,  
and International Center for Young Scientists,  
National Institute for Materials Science, 1-1 Namiki,  
Tsukuba, Ibaraki 305-0044, Japan

Received January 12, 2007

Revised Manuscript Received March 21, 2007

Carbon-based materials have received enduring attention from various scientists due to their unique properties, diverse morphology, and wide applications. Fullerene (C<sub>60</sub>), the most interesting candidate in the carbon family, has peculiar structural characteristics over other members. Indeed, it has various applications like other carbon materials in fields such as sensors, catalysis, and optical devices. The recent development in one-dimensional nanostructural materials with assorted morphology like nanotube, nanorods, nanoplates, etc., has further enhanced the utility of these carbon materials.

The self-slow-aggregation of C<sub>60</sub> molecules into a small cluster in the pure solvent medium is well-known.<sup>1,2</sup> On the basis of this, various crystalline C<sub>60</sub> crystals were grown in different solvents with dissimilar structure and diverse shapes.<sup>3–5</sup> The nature of the solvent plays a major role in the cluster structure, and the various mechanistic approaches for cluster formation are described.<sup>6</sup> In the earlier reported literature, the obtained C<sub>60</sub> crystals are a few micrometers or millimeters in diameter and crystallinity is stabilized by the solvent molecule. More recently, the synthesis of C<sub>60</sub> nanotubes or nanowhiskers has created an enormous amount of expectation due to the nanosize and the tubular morphology similar to that of carbon nanotubes. Unlike other carbon materials, the C<sub>60</sub> nanotube has solubility in various organic solvents, which adds supplementary advantages to the exploitation of C<sub>60</sub> nanotubes as a removable template.<sup>7</sup>

Various synthetic strategies have been introduced for the preparation of C<sub>60</sub> nanowhiskers (or) nanotubes.<sup>8–10</sup> In our earlier study, we introduced liquid–liquid interfacial precipitation of C<sub>60</sub> and C<sub>70</sub> nanowhiskers using toluene or *m*-xylene and isopropyl alcohol (IPA) interface.<sup>11–13</sup> It is believed that the porous nanowhiskers preparation could be possible only by our interfacial preparation method. Pursuing our efforts toward the finding of a better solvent system for the synthesis of porous C<sub>60</sub> nanowhiskers, we have evaluated

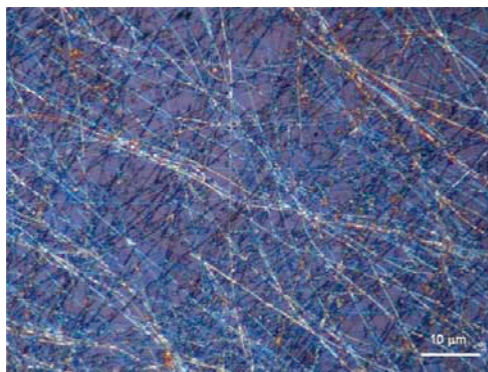


Figure 1. Optical microscopic image of C<sub>60</sub> nanowhiskers.

various combinations of solvents. Finally, the formation of porous C<sub>60</sub> nanowhiskers have been successfully obtained by mixing of different ratios (v/v) of C<sub>60</sub> saturated benzene and IPA. Before mixing, the solutions were cooled to 5 °C and the IPA was added slowly to the C<sub>60</sub>-saturated benzene solution. After the addition, the solution was ultrasonicated for 1 min at 5 °C in an ultrasonic water bath. The resulting mixture was kept in an incubator at 5 °C for 24 h. The optical microscopic image of the C<sub>60</sub> nanowhiskers produced at the benzene–IPA interface is shown in Figure 1. Very thin nanowhiskers few hundred micrometers in length were observed. This can also be seen from the microscopic image that the nanowhiskers are uniform in size throughout the length of the tube. Unlike the nonporous nanowhiskers reported earlier by our group and other researchers, in the present case, nanowhiskers with very fine pores have been observed. Although the pore size and shape vary, they were insignificant compared to the whole view.

The morphology of the prepared C<sub>60</sub> nanowhiskers has been further analyzed by FE-SEM analysis. Figure 2 shows the FE-SEM images of the prepared porous nanowhiskers at different magnification. Very long C<sub>60</sub> nanowhiskers (more than 100 micrometers) with uniform size were observed in the mesh. The average size of nanowhiskers is around 100 nm in diameter. However, because of the Pt sputtering, the morphology of pores on the surface could not be seen clearly.

Figure 3 shows a representative set of scanning transmission electron microscopy (STEM) images of the C<sub>60</sub> nanowhiskers prepared at the benzene–IPA interface. The observed sample contains both the tubular and nontubular C<sub>60</sub>

\* Corresponding author. E-mail: MARAPPAN.Sathish@nims.go.jp.

<sup>†</sup> Fuel Cells Materials Center, National Institute for Materials Science.

<sup>‡</sup> International Center for Young Scientists, National Institute for Materials Science.

- (1) Ying, Q.; Marecek, J.; Chu, B. *Chem. Phys. Lett.* **1994**, *219*, 214–218.
- (2) Ghosh, H. N.; Sapre, A. V.; Mittal, J. P. *J. Phys. Chem.* **1996**, *100*, 9439–9443.
- (3) Pekker, S.; Faigel, G.; Fodor-Csorba, K.; Gra'na'sy, L.; Jakab E.; Tegze, M. *Solid State Commun.* **1992**, *83*, 423–426.
- (4) Meidine, M. F.; Hitchcock, P. B.; Kroto, H. W.; Taylor, R.; Walton, D. R. M. *J. Chem. Soc., Chem. Commun.* **1992**, 1534–1537.
- (5) Graja, A.; Swietlik, R. *Synth. Met.* **1995**, *70*, 1417–1418.
- (6) Bezmel'nitsyn, V. N.; Eletskii, A. V.; Stepanov, E. V. J. In *Progress in Fullerene Research*; Kuzmany, H., Ed.; World Scientific: Singapore, 1994; p 45.
- (7) Minato, J.; Miyazawa, K. *J. Mater. Res.* **2006**, *21*, 539–534.

- (8) (a) Wang, L.; Liu, B.; Yu, S.; Yao, M.; Liu, D.; Hou, Y.; Cui, T.; Zou, G.; Sundqvist, B.; You, H.; Zhang, D.; Ma, D. *Chem. Mater.* **2006**, *18*, 4190–4194. (b) Wang, L.; Liu, B.; Liu, D.; Yao, M.; Hou, Y.; Yu, S.; Cui, T.; Li, D.; Zou, G.; Iwasiewicz, A.; Sundqvist, B. *Adv. Mater.* **2006**, *18*, 1883–1888.
- (9) Liu, H.; Li, Y.; Jiang, L.; Luo, H.; Xiao, S.; Fang, H.; Li, H.; Zhu, D.; Yu, D.; Xu, J.; Xiang, B. *J. Am. Chem. Soc.* **2002**, *124*, 13370–3371.
- (10) Jin, Y.; Curry, R. J.; Sloan, J.; Hatton, R. A.; Chong, L. C.; Blanchard, N.; Stolojan, V.; Kroto, H. W.; Silva, S. R. P. *J. Mater. Chem.* **2006**, *16*, 3715–3720.
- (11) Miyazawa, K.; Kuwasaki, Y.; Obayashi, A.; Kuwabara, M. *J. Mater. Res.* **2002**, *17*, 83–88.
- (12) Miyazawa, K.; Hamamoto, K.; Nagata, S.; Suga, T. *J. Mater. Res.* **2003**, *18*, 1096–1103.
- (13) Minato, J.; Miyazawa, K. *Carbon* **2005**, *43*, 2837–2841.

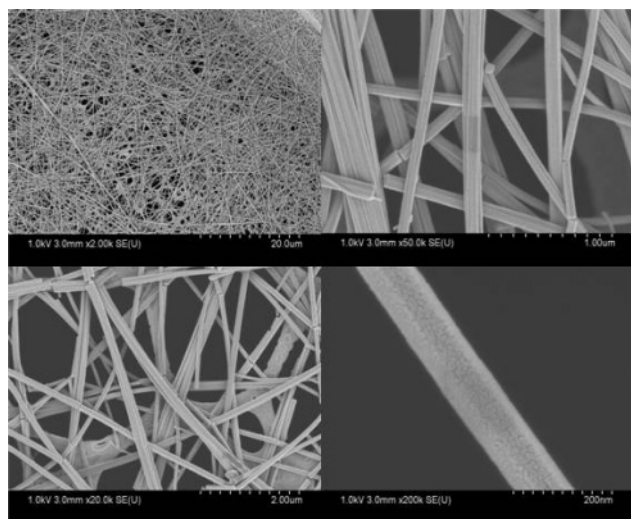


Figure 2. FE-SEM images of platinum sputtered  $C_{60}$  nanowhiskers.

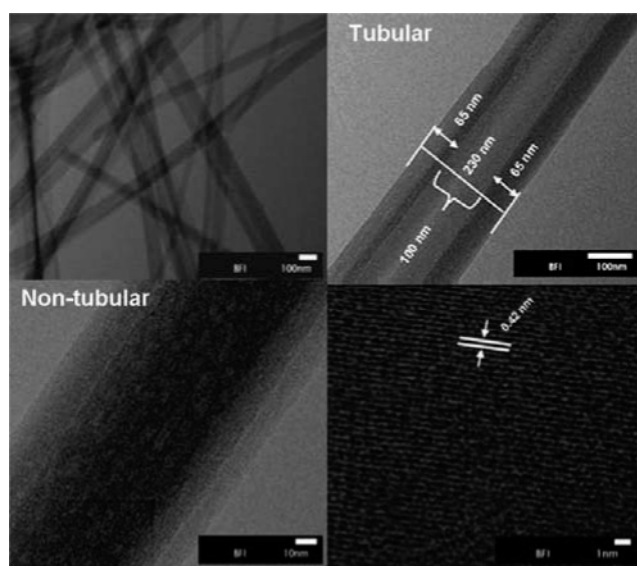


Figure 3. STEM images of  $C_{60}$  nanowhiskers.

nanowhiskers in the range of 100–300 nm in diameter. In the case of tubular nanowhiskers, the inner diameter of the tube is  $\sim 100$  nm and the wall thickness is 65 nm. Regardless of the inner diameter, the wall thickness is found to be constant in the range of 65–75 nm for the other tubular nanowhiskers. In the case of nontubular nanowhiskers, a very thin layer of amorphous surface was found. The size of the nontubular nanowhiskers was found to be smaller when compared to tubular nanowhiskers. A clear lattice fringing has been observed for the nontubular nanowhiskers with a lattice plane spacing of 0.42 nm. This obtained value has good concordance with the  $d$  value of the (311) plane. The length of the nanowhiskers is in the range of a few hundred micrometers.

The TEM images of the nanowhiskers are shown in Figure 4. The fine pores on the wall surface of the nanowhiskers are clearly visible (indicated by red circle). The observed pores are not uniform in size and shape. It is presumed that during the formation process of  $C_{60}$  nanowhiskers, the solvent molecule occupies the space inside the pores of the tubes. The solvent molecules that present inside the tubes get

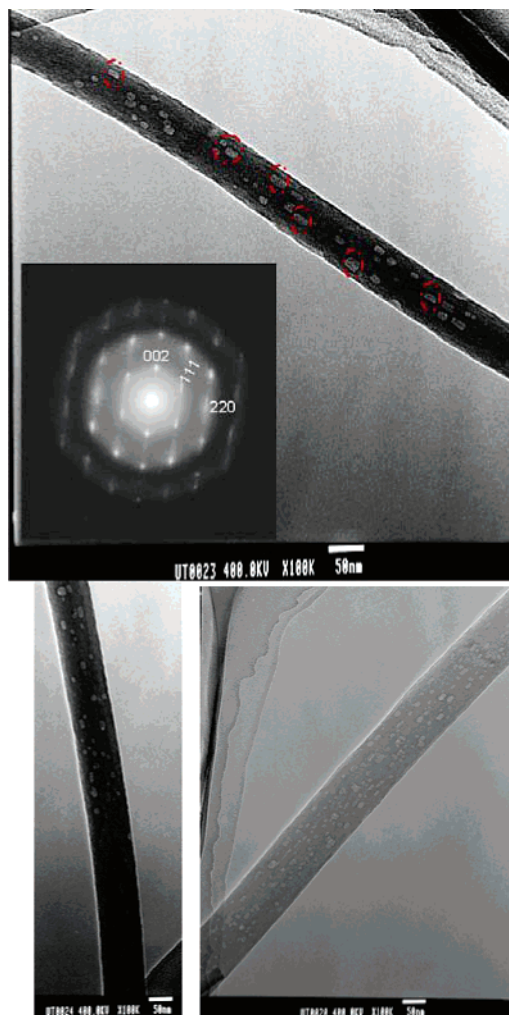
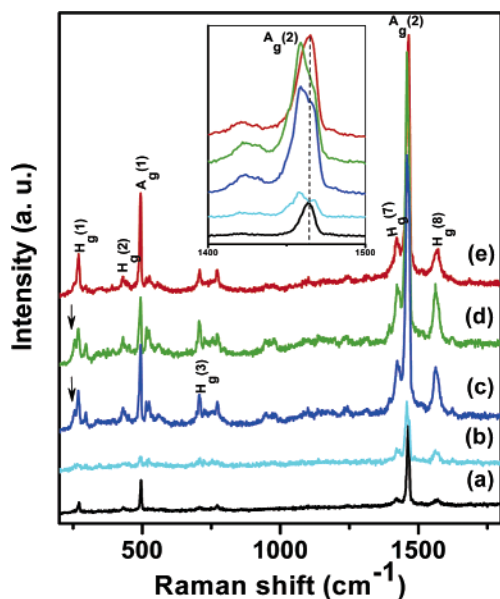


Figure 4. TEM images of nontubular porous  $C_{60}$  nanowhiskers.

evaporated during the drying process. The evaporation of solvent makes the pores on the walls of the nanowhiskers. It is speculated that the solvent-evaporation process has a crucial role in the structure direction and leads to tubular and nontubular nanowhisker formation. The nanowhiskers that are smaller in size ( $< 100$  nm) become nontubular and the nanowhiskers with a larger size ( $> 100$  nm) surmount the tubular structure. Certainly, the observed porous nanowhiskers with a size less than 100 nm are nontubular, which supports the above speculation that solvent evaporation in the small nanowhiskers makes nontubular nanowhiskers. However, there is no comprehensible evidence for the formation of tubular and nontubular nanowhiskers. The formation of pores has been further confirmed by the observed higher specific surface area of  $376 \text{ m}^2/\text{g}$ , whereas the specific surface area of pristine  $C_{60}$  powder is  $20 \text{ m}^2/\text{g}$ .

The inset of Figure 4 shows the selected area electron diffraction pattern of porous  $C_{60}$  nanowhiskers, the acquired pattern shows that the nanowhiskers are face-centered cubic in structure.<sup>11</sup> The crystalline nature has been further confirmed by X-ray diffraction pattern (XRD) analysis. The XRD pattern (see the Supporting Information) of room-temperature dried  $C_{60}$  nanowhiskers shows three major peaks at  $2\theta$  values of 10.7, 17.6, and 20.6 corresponding to (111), (220), and (311) plane reflections, respectively. The obtained XRD pattern can be indexed for the fcc crystal system.<sup>14,11</sup>





**Figure 5.** Raman spectroscopy of (a) pristine  $C_{60}$  and porous  $C_{60}$  nanowhiskers prepared at (b) 1:9, (c) 1:8, (d) 1:6, and (e) 1:4 benzene:IPA ratios.

However, the reflection corresponding to the (200) plane was not observed for the porous nanowhiskers. Likewise, the absence of the 200 reflection is typical for pristine fcc  $C_{60}$  crystals.<sup>15</sup>

To understand the effect of solvent ratio on the  $C_{60}$  nanowhisker formation, the  $C_{60}$ -saturated benzene to IPA ratio has been varied between 1:3 to 1:12 with 1 mL intervals. The growth of nanowhiskers has been observed for all ratios up to 1:9; however, above this ratio, formation of nanowhiskers was not observed even after 1 week's time. It is commonly accepted that the solvent ratio has a crucial role in the growth of nanowhiskers. Also, the effect of temperature on the growth rate has been studied at 5, 10, 15, and 25 °C for the 1:4.5 ratio of  $C_{60}$ -saturated benzene and IPA. Interestingly, the effects of temperature on the growth of the  $C_{60}$  nanowhiskers have been observed at the interface. The growth rate has an inverse dependence with increase in temperature. As the temperature increases, the growth time also increases and the yield of the nanowhiskers decreases gradually. However, there is no formation of nanowhiskers at room temperature (25 °C), even after a very long time. Regardless of the temperature and solvent ratio, the obtained nanowhiskers show very fine and narrow pores in nontubular morphology.

The  $C_{60}$  nanowhiskers prepared at different ratios of the solvent have been scrutinized using Raman spectroscopy. Figure 5 shows the Raman spectra of the nanowhiskers and pristine  $C_{60}$  powder.

The observed Raman lines at 267, 429, 494, 707, 1423, 1459, and 1562  $cm^{-1}$  are attributed to  $H_g(1)$ ,  $H_g(2)$ ,  $A_g(1)$ ,  $H_g(3)$ ,  $H_g(7)$ ,  $A_g(2)$ , and  $H_g(8)$  modes for  $C_{60}$  molecules,<sup>16</sup> respectively. Among the Raman active lines, the most significant one is the line at 1469  $cm^{-1}$ , which corresponds to the “pentagonal pinch” mode or  $A_g(2)$  mode. This has been used extensively as an analytical probe for the structural and electronic properties of  $C_{60}$  molecules.<sup>16</sup> This mode is very susceptible to intermolecular bonding. Although there is no

significant difference between Raman spectra of nanowhiskers prepared with different solvent ratios, a noticeable peak shift for the  $A_g(2)$  mode has been observed at 1459  $cm^{-1}$  for the nanowhiskers compared to the pristine  $C_{60}$  powder. Figure 5 (inset) shows the Raman lines of the  $A_g(2)$  mode for the nanowhiskers and pristine  $C_{60}$ . A very clear downshift was observed for the porous nanowhiskers. Indeed, the shift in the peak position is negligible for the nanowhiskers prepared with a lower solvent ratio (1:4), but at a higher solvent ratio (1:6 and above), the shift is very significant. The observed downshift from 1469  $cm^{-1}$  for the nanowhiskers can be attributed to the polymerization of  $C_{60}$  molecules in the nanowhiskers.<sup>17</sup> A similar observation in the downshift has been observed for the photoassisted polymerization of  $C_{60}$  solid.<sup>18,19</sup> Hence, it is speculated that the polymerization possibly will occur during the laser irradiation, which is used for the Raman spectroscopic measurements (Figure 5). In addition, the peak around the 267  $cm^{-1}$  shows a clear splitting (shown by arrow in Figure 5) in the lower-frequency region for the nanowhiskers prepared at 1:6, 1:8, and 1:9 ratios. The peak splitting hints to the polymerization  $C_{60}$  molecule in the nanowhiskers. However, this splitting may also occur because of the good crystalline nature of the nanowhiskers. Thus, detailed investigation is necessary to account for the above splitting in the Raman lines.

In summary, we have succeeded in the preparation of porous  $C_{60}$  nanowhiskers using the liquid–liquid interfacial precipitation method. The prepared nontubular nanowhiskers contain nanopores over the wall surface. The porous nanowhiskers show higher specific surface area than pristine  $C_{60}$  powder. The preparation of porous tubular nanowhiskers is our ultimate aim, as a template for the preparation of various metal/metal oxide nanowire or nanotubes. The electron diffraction and XRD pattern reveals the fcc crystalline nature of the prepared porous nanowhiskers. Raman spectroscopic studies on the porous nanowhiskers show the polymerization of  $C_{60}$  molecules (due to laser light irradiation). We are currently exploiting the nanoporous nanowhiskers for various applications, particularly as an anode material for the fuel cell and template for the preparation of metal-oxide nanostructures.

**Acknowledgment.** The part of this research was financially supported by a Grant in Aid for Scientific Research of the Ministry of Education, Culture, Sports, Science and Technology of Japan (Projects 17201027 and 17651076).

**Supporting Information Available:** Experimental details and XRD pattern. This material is available free of charge via the Internet at <http://pubs.acs.org>.

CM070114A

- (14) Gupta, V.; Scharff, P.; Miura, N. *Mater. Lett.* **2006**, *60*, 3156–3159.
- (15) Fischer, J. E.; Heiney, P. A.; Luzzi, D. E.; Cox, D. E. In *Fullerenes*; Hammond, G. S., Kuck, V. J., Eds.; American Chemical Society: Washington, D.C., 1992; p 55–69.
- (16) Kuzmany, H.; Pfeiffer, R.; Hulman, M.; Kramberger, C. *Philos. Trans. R. Soc. London, Ser. A* **2004**, *362*, 2375–2406.
- (17) Martin, M. C.; Koller, D.; Rosenberg, A.; Kendziora, C.; Mihaly, L. *Phys Rev. B* **1995**, *51*, 3210–3213.
- (18) Tachibana, M.; Kobayashi, K.; Uchida, T.; Kojima, K.; Tanimura, M.; Miyazawa, K. *Chem. Phys. Lett.* **2003**, *374*, 279–285.
- (19) Rao, A. M.; Eklund, P. C.; Venkatswaran, U. D.; Tucker, J.; Duncan, M. A.; Bendele, G. M.; Nuñez-Regueiro, M.; Bashkin, I. O.; Ponyatovsky, E. G.; Morovsky, A. P. *Appl. Phys. A* **1997**, *64*, 231–239.